Comput Mech (2005) 37: 2–14
DOI 10.1007/s00466-005-0692-3

ORIGINAL PAPER

C. W. Chen · D. L. Young · C. C. Tsai · K. Murugesan

The method of fundamental solutions for inverse 2D Stokes problems

Received: 25 May 2004 / Accepted: 15 December 2004 / Published online: 4 June 2005

Abstract A numerical scheme based on the method of fundamental solutions is proposed for the solution of two-dimensional boundary inverse Stokes problems, which involve over-specified or under-specified boundary conditions. The coefficients of the fundamental solutions for the inverse problems are determined by properly selecting the number of collocation points using all the known boundary values of the field variables. The boundary points of the inverse problems are collocated using the Stokeslet as the source points. Validation results obtained for two test cases of inverse Stokes flow in a circular cavity, without involving any iterative procedure, indicate the proposed method is able to predict results close to the analytical solutions. The effects of the number and the radius of the source points on the accuracy of numerical predictions have also been investigated. The capability of the method is demonstrated by solving different types of inverse problems obtained by assuming mixed combinations of field variables on varying number of under- and over-specified boundary segments.

Keywords Method of fundamental solutions · Stokeslet · Inverse problem · Circular cavity · Meshless numerical method

C. W. Chen · D. L. Young (✉) · K. Murugesan
Department of Civil Engineering & Hydrotech Research Institute, National Taiwan University, Taipei, Taiwan
E-mail: dlyoung@ntu.edu.tw
Fax: +886-2-23626114

C. C. Tsai
Department of Information Technology, Toko University, Chia-Yi County, Taiwan

1 Introduction

The method of fundamental solutions (MFS) is one of the most promising meshless numerical schemes to solve boundary value problems when the fundamental solution of the differential equation in question exists. The approximate numerical solution for a given problem is obtained by a linear combination of the fundamental solutions of source points that are located on an artificial boundary. The MFS retains the advantages of the boundary element method (BEM) in that the solution procedure does not require the discretization of the interior domain, but also overcomes the problem of singularity and avoids the boundary element integrations. Since the MFS does not require mesh discretization of the interior region of the computational domain, compared to the domain discretization methods, a significant amount of computational effort and time is saved. Fairweather & Karageorghis [1], Fairweather et al. [2], and Golberg and Chen [3] have discussed in detail the advantages of the MFS over the domain discretization methods, along with an exhaustive survey of the MFS over the past three decades. Due to its simplicity in implementation the MFS has been applied successfully to deal with different types of boundary value problems as discussed in References [1–4].

As far as the Stokes flow problems are concerned, Tsai et al. [5] utilized the MFS to solve Stokes flow problems based on the Laplacian and the velocity-vorticity formulation. Recently, Tsai [6], and Alves and Silvestre [7] employed the MFS to solve Stokes equations using Stokeslet as source points placed randomly outside the domain.

Applications of the MFS for the solution of well-posed Stokes equations are straight forward [6, 7]. However when the problem is ill-posed with over-specified and under-specified boundary conditions, the numerical procedure generally involves either an iterative numerical scheme or a regularization technique. Agoshkov et al. [8] used an iterative solution procedure

to numerically solve a boundary inverse Stokes problem. When boundary methods such as the BEM or the MFS is used for the solution of inverse boundary value problems, the resulting system of algebraic equations is generally ill-conditioned and the solution has to be regularized using some regularization functionals. Farcas et al. [9] used the dual reciprocity boundary element method to solve an inverse Poisson equation. They employed the Tikhonov regularization technique to overcome the resulting ill-conditioned equations. Zeb et al. [10, 11] also used the BEM associated with a similar regularization technique to solve inverse problems that involve Stokes equations [10] and biharmonic equations [11]. Marin and Lesnic [12] applied the MFS for the solution of a Cauchy problem associated with two-dimensional linear elasticity. Marin [13] extended this scheme to solve a Cauchy problem involving three-dimensional Helmholtz-type equations. The Tikhonov regularization technique was used to circumvent the ill-conditioned equations of the previous two works.

In the present work, the MFS based on the Stokeslet is devised to solve certain types of inverse Stokes flow problems, without using either an iterative procedure or a regularization technique as done in other works [8–13]. The coefficients used in the fundamental solution of the MFS do not pose any constraint on the specification of all the flow variables on the computational boundary, thus the MFS can be used to determine the boundary values of the field variables on the under-specified and over-specified regions. After verifying the accuracy of the boundary values, the field variables in the interior domain can be determined. The proposed method is demonstrated by applying it to different types of inverse Stokes flows in a circular cavity subjected to under-specified and over-specified boundary conditions. In the following sections, the governing equations used, the numerical procedure followed and the results obtained are discussed.

2 Governing equations and Stokeslet

The governing equations for Stokes flow are represented in primitive variable form as follows:
Continuity equation

$$\nabla\cdot\vec{u} = 0 \tag{1}$$

Momentum equation

$$-\nabla p + \mu\nabla^2\vec{u} = 0 \tag{2}$$

where p is the pressure, $\vec{u} = (u, v)$ is the 2D velocity vector and μ is the absolute or dynamic viscosity of the fluid. The solution of the field variables must be obtained in a computational domain Ω enclosed by a boundary Γ. When the boundary conditions for velocity or pressure are specified on Γ the problem becomes well-posed and can be solved using a suitable numerical scheme. The use of the MFS to solve such direct problems is well established [6, 7].

In the case of Stokes flows, the Stokeslet has been used as source points in the present work, since the Stokeslet is the fundamental solution of the Stokes equations. The Stokeslet represents the velocity and pressure due to a concentrated point force acting in a fluid continuum. In other words, the Stokeslet satisfies the following equation [14]:

$$-\nabla p^* + \mu\nabla^2\vec{u}^* = -\vec{b}\delta(\vec{x} - \vec{x}_0) \tag{3}$$

where $\vec{b} = (b^x, b^y)$ is the magnitude of the applied force, $\delta(\vec{x} - \vec{x}_0)$ is the well-known Dirac delta function, $\vec{x} = (x, y)$ is the position of the field point and $\vec{x}_0 = (x_0, y_0)$ is the location of the source point.

By solving the fundamental solutions of the Eqs. (1) and (3), the Stokeslet can be well defined. For the case of two-dimensional flow field, the Stokeslet is given as follows:

$$u^* = \frac{1}{8\pi\mu}\left[b^x\left(-2\ln(r) + \frac{2\widehat{x}^2}{r^2} - 3\right) + b^y\left(\frac{2\widehat{x}\widehat{y}}{r^2}\right)\right] \tag{4}$$

$$v^* = \frac{1}{8\pi\mu}\left[b^x\left(\frac{2\widehat{x}\widehat{y}}{r^2}\right) + b^y\left(-2\ln(r) + \frac{2\widehat{y}^2}{r^2} - 3\right)\right] \tag{5}$$

$$p^* = \frac{1}{2\pi}\left[b^x\left(\frac{\widehat{x}}{r^2}\right) + b^y\left(\frac{\widehat{y}}{r^2}\right)\right] \tag{6}$$

$$\zeta^* = \frac{1}{2\pi\mu}\left[b^x\left(\frac{\widehat{y}}{r^2}\right) - b^y\left(\frac{\widehat{x}}{r^2}\right)\right] \tag{7}$$

$$\psi^* = \frac{1}{8\pi\mu}[-b^x\widehat{y}(2\ln(r) + 1) + b^y\widehat{x}(2\ln(r) + 1)] \tag{8}$$

where $r = |\vec{x} - \vec{x}_0|$ is the distance between the source point and the field point, $\widehat{x} = x - x_0$, $\widehat{y} = y - y_0$ are the x- and y-coordinate differences between these two points, and ζ^* and ψ^* represent the vorticity and stream function, which are defined by $\zeta^* = \frac{\partial v^*}{\partial x} - \frac{\partial u^*}{\partial y}$ and $u^* = \frac{\partial \psi^*}{\partial y}$ & $v^* = -\frac{\partial \psi^*}{\partial x}$, respectively. For two-dimensional problems Eqs. (4)–(8) denote the Stokeslet. The following section illustrates that the MFS can be exploited to solve inverse Stokes problems directly without using any iterative scheme or a regularization technique.

3 Numerical solutions of inverse problems using MFS

Let us consider a flow domain consisting of two boundary segments Γ_I, and Γ_{II} as shown in Fig. 1a. We seek the numerical solutions of the flow variables in the Domain Γ. In order to avoid the singular problems in the MFS induced by the Stokeslet, the source points are placed on an artificial boundary at a distance away from the surrounding boundary of the computational domain, as illustrated in Fig. 1b. The Stokeslet is assumed to be located on an artificial boundary with different strengths. After considering the strengths generated by the Stokeslet on the source points, the expressions for the velocities can be represented as

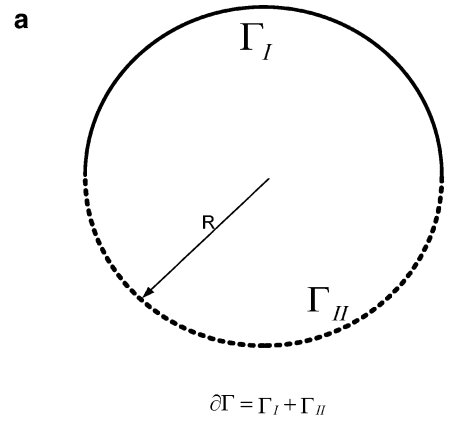

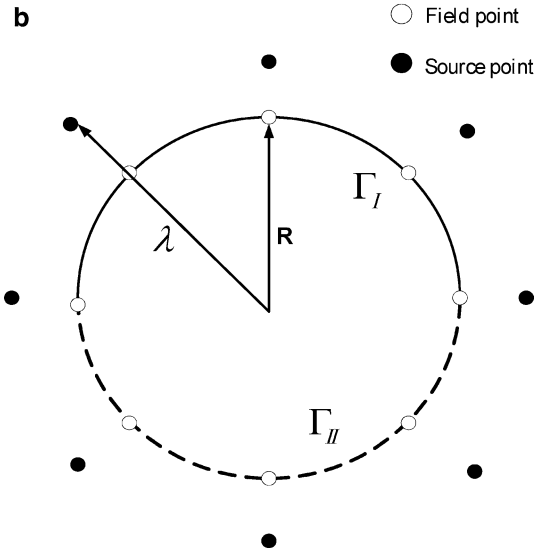

Fig. 1 Schematic diagram for **a** under-specified (Γ_{II}) and over-specified (Γ_I) boundary **b** distributions of source points and boundary points

$$u(\vec{x}_i) = \frac{1}{8\pi\mu}\left[\sum_{j=1}^{N}\alpha_j^x\left(-2\ln(r_{ij}) + \frac{2(x_i - x_j)^2}{r_{ij}^2} - 3\right) + \sum_{j=1}^{N}\alpha_j^y\left(\frac{2(x_i - x_j)(y_i - y_j)}{r_{ij}^2}\right)\right] \quad (9)$$

$$v(\vec{x}_i) = \frac{1}{8\pi\mu}\left[\sum_{j=1}^{N}\alpha_j^x\left(\frac{2(x_i - x_j)(y_i - y_j)}{r_{ij}^2}\right) + \sum_{j=1}^{N}\alpha_j^y\left(-2\ln(r_{ij}) + \frac{2(y_i - y_j)^2}{r_{ij}^2} - 3\right)\right] \quad (10)$$

where N is the number of source points, α_j^x and α_j^y are the coefficients of the fundamental solutions in the x and y directions respectively. After obtaining the values of the above coefficients, the pressure, vorticity and stream function components can be determined using the following equations:

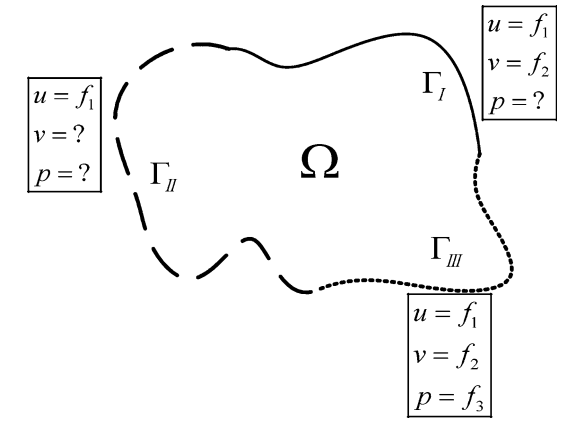

Fig. 2 Schematic diagram for inverse Stokes problem with multiple boundary segments

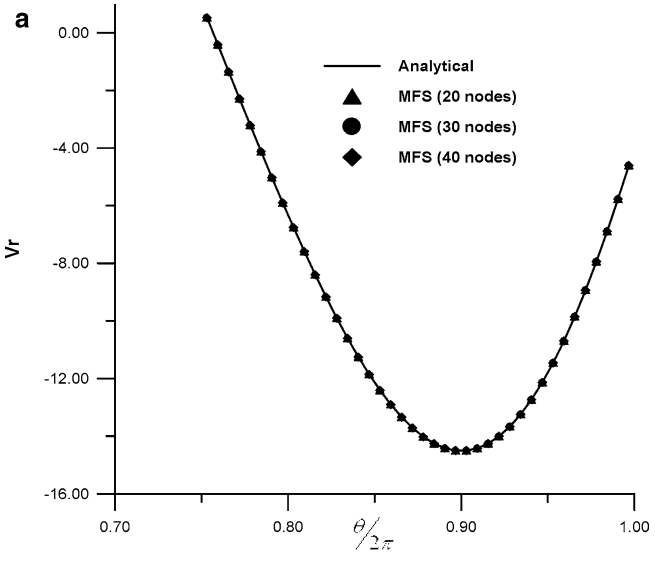

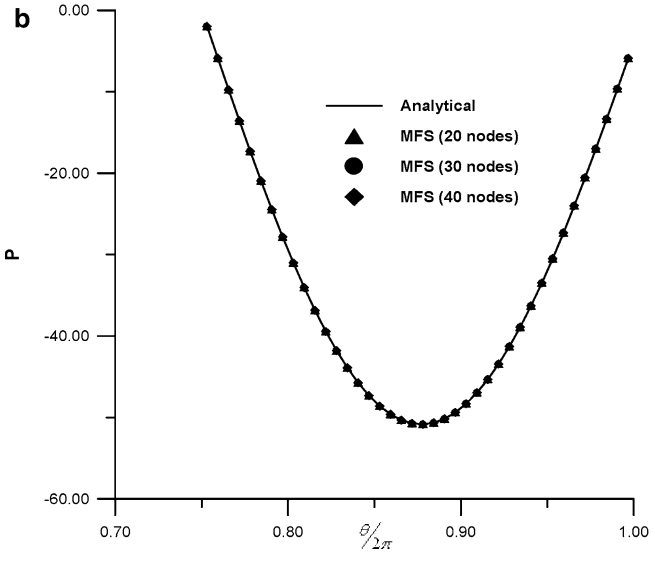

Fig. 3 Comparison with analytical solutions and effect of number of boundary points on the results of **a** $v_\Gamma|_{\Gamma_{II}}$ and **b** $p|_{\Gamma_{II}}$, on the under-specified boundary

Table 1 Comparison with analytical solutions and effect of number of boundary points on v_r and P on under-specified boundary

$\theta/2\pi$	V_r				The unknown pressure (P)			
	Analytical	MFS (20 nodes)	MFS (30 nodes)	MFS (40 nodes)	Analytical	MFS (20 nodes)	MFS (30 nodes)	MFS (40 nodes)
0.76250	−0.88416	−0.88403	−0.88416	−0.88416	−7.82269	−7.82242	−7.82271	−7.82269
0.78750	−4.57658	−4.57681	−4.57659	−4.57658	−22.72533	−22.72649	−22.72542	−22.72533
0.81250	−8.00087	−8.00088	−8.00084	−8.00087	−35.47186	−35.47571	−35.47189	−35.47186
0.83750	−10.93521	−10.93424	−10.93523	−10.93521	−44.85831	−44.86273	−44.85800	−44.85831
0.86250	−13.13414	−13.13360	−13.13419	−13.13414	−50.00683	−50.00676	−50.00660	−50.00683
0.88750	−14.34648	−14.34670	−14.34643	−14.34648	−50.45066	−50.44541	−50.45097	−50.45066
0.91250	−14.35087	−14.35166	−14.35088	−14.35087	−46.17887	−46.17286	−46.17913	−46.17887
0.93750	−13.00295	−13.00388	−13.00293	−13.00295	−37.63664	−37.63429	−37.63659	−37.63664
0.96250	−10.28399	−10.28396	−10.28399	−10.28399	−25.68102	−25.68276	−25.68093	−25.68102
0.98750	−6.33852	−6.33822	−6.33853	−6.33852	−11.49652	−11.49879	−11.49652	−11.49652
Max.error (%)		9.75 E−02	5.10 E−03	1.95 E−06		6.01 E−01	3.11 E−02	2.30 E−05

$$p(\vec{x}_i) = \frac{1}{2\pi}\left[\sum_{j=1}^{N}\alpha_j^x\left(\frac{x_i - x_j}{r_{ij}^2}\right) + \sum_{j=1}^{N}\alpha_j^y\left(\frac{y_i - y_j}{r_{ij}^2}\right)\right] \tag{11}$$

$$\zeta(\vec{x}_i) = \frac{1}{2\pi\mu}\left[\sum_{j=1}^{N}\alpha_j^x\left(\frac{y_i - y_j}{r_{ij}^2}\right) - \sum_{j=1}^{N}\alpha_j^y\left(\frac{x_i - x_j}{r_{ij}^2}\right)\right] \tag{12}$$

$$\psi(\vec{x}_i) = \frac{1}{8\pi\mu}\left[\sum_{j=1}^{N}\alpha_j^x\Big(-(y_i - y_j)\big[2\ln(r_{ij}) + 1\big]\Big) + \sum_{j=1}^{N}\alpha_j^y\Big((x_i - x_j)\big[2\ln(r_{ij}) + 1\big]\Big)\right] \tag{13}$$

Finally when all the coefficients are determined, the computation of the flow variables at the interior domain can be obtained directly from Eqs. (9)–(13). It is worthwhile to observe that if the velocity boundary conditions are well posed, there is no need to specify the boundary conditions of pressure or vorticity. This is evidenced from the examination of Eqs. (9)–(13) by judging the fact that the determination of the coefficients of α_j^x and α_j^y can be obtained from any two field variables among the u, v velocity, pressure, vorticity or stream function. This formulation is ideal for the inverse Stokes problems since by this method it is very easy to treat the under- and over-specified boundary conditions for any kind of field variables. Thus the iterative and regularization procedures are avoided.

To illustrate the numerical details of the MFS, a flow domain with three multiple boundary segments Γ_I, Γ_{II} and Γ_{III}, subjected to under-specified and over-specified boundary conditions is considered as shown in Fig. 2. In the numerical procedure, the same number of equations is specified to solve the unknown coefficients, which depend only on the dimensionality of the computational domain and the number of collocation points. Herein, the collocation points should be chosen to include all the available boundary values of the flow variables. In other words, all those known boundary values on the under-specified and over-specified boundary segments are used to determine the coefficients of the fundamental solution in order to satisfy the physics underlying the problem.

Let us consider M field points on each of the three boundary segments for the inverse Stokes problem shown in Fig. 2. For each known field variable on a boundary segment, M equations will be obtained for the corresponding field variable. The over-specified and under-specified boundary values on all the three boundary segments constitute the load vector for the coefficient matrix. Thus the final matrix equations to determine the coefficients α_j^x and α_j^y are obtained from

$$[A_{ij}]\begin{Bmatrix}[\alpha_j^x]\\ [\alpha_j^y]\end{Bmatrix} = \begin{Bmatrix} u_{i\Gamma_I}\\ v_{i\Gamma_I}\\ u_{i\Gamma_{II}}\\ u_{i\Gamma_{III}}\\ v_{i\Gamma_{III}}\\ p_{i\Gamma_{III}}\end{Bmatrix}$$

where $j = 1, \ldots, 3M, \quad i = 1, \ldots, M.$ (14)

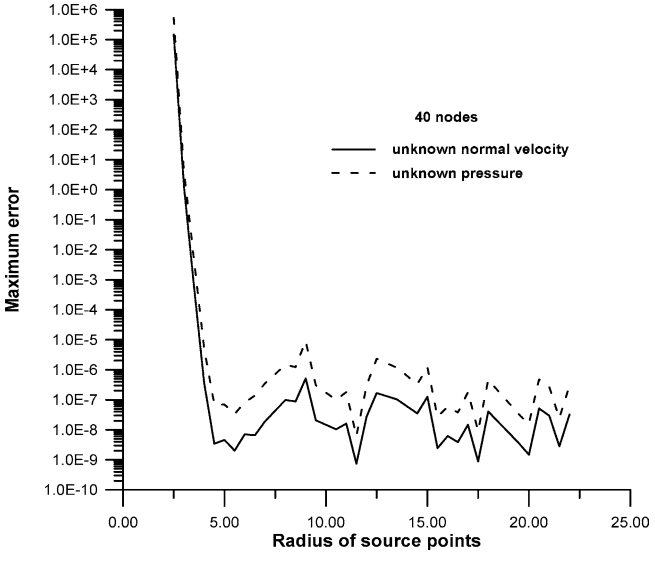

Fig. 4 Variation of maximum error with radius of source points for 40 boundary points

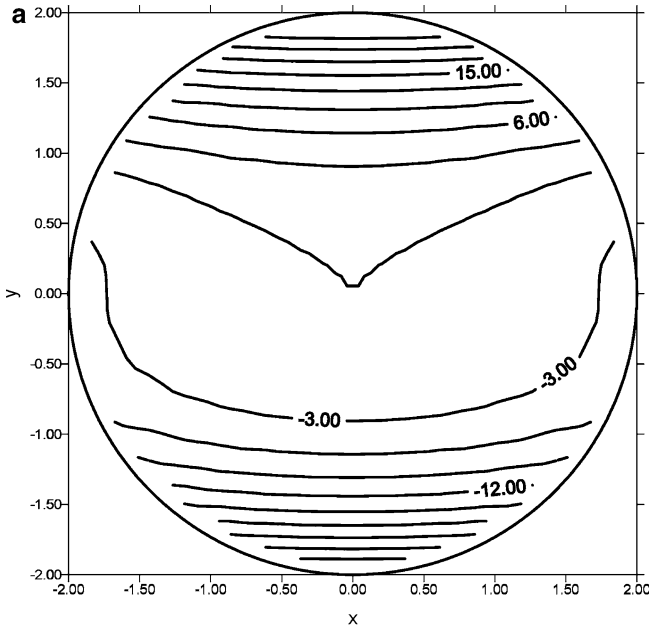

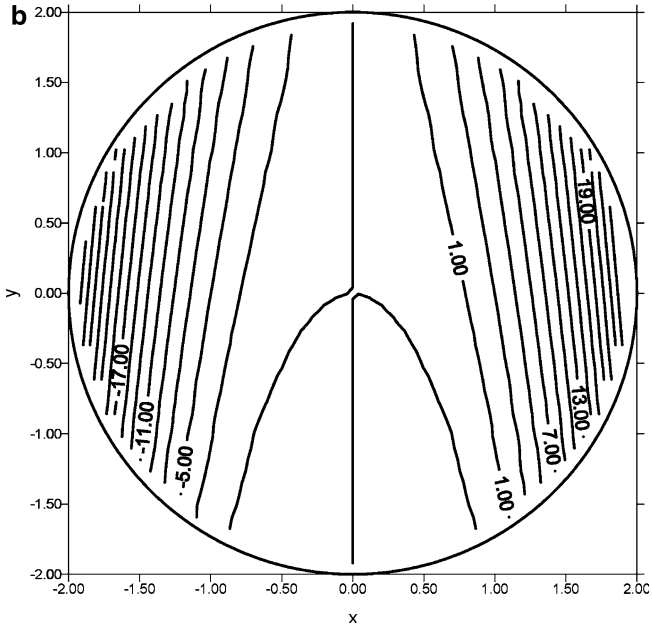

Fig. 5 The numerical results and corresponding analytical solutions for **a** the interior velocity (u) **b** the interior velocity (v)

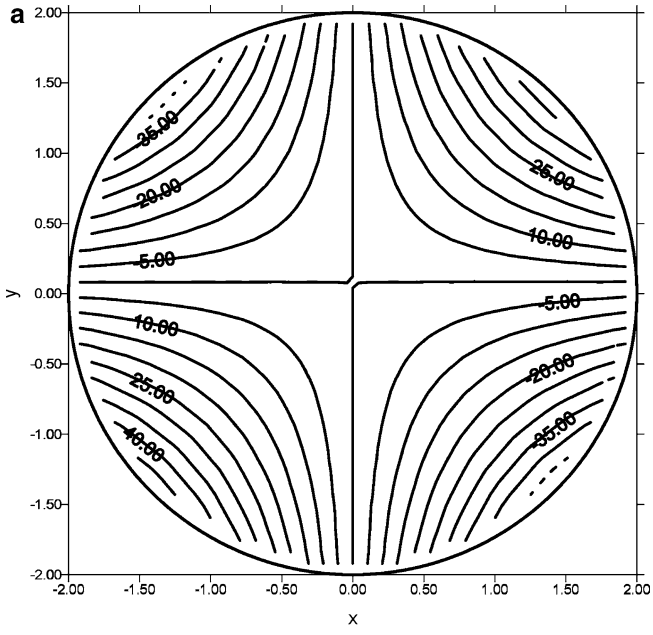

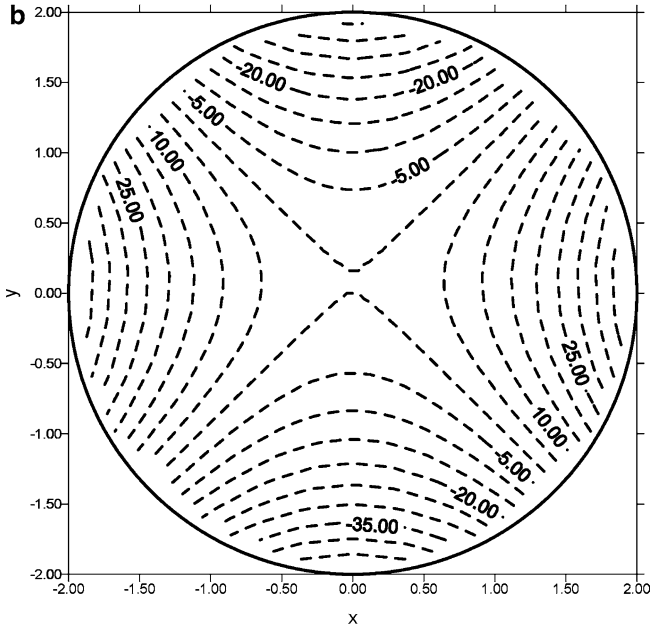

Fig. 6 The numerical results and corresponding analytical solutions for **a** the interior pressure (P) and **b** the interior vorticity (ς)

where α_j^x and α_j^y are the coefficients of the fundamental solution of the field variables. By collocating all the source points on the known boundary conditions, the number of equations to be solved is computed. Once the coefficients α_j^x and α_j^y are determined, the under-specified boundary values of the flow field variables are computed using the respective expressions. These values are treated as the internal domain values just coinciding with the boundary. Numerically, it is found that the resulting linear system can be solved for all numerical experiments once the source points are not located too near the boundary points.

To study the sensitivity of the accuracy for different locations of the source points on the fictitious boundary, we define a radius of source points, λ, with the origin at the geometric center of the computational domain. The schematic diagram is shown in Fig. 1b. Numerical experiments reveal that to obtain accurate solutions, there is a wide range of the radius of the source points. If the source points of the fictitious boundary are too close to the boundary collocation points, the numerical accuracy will be jeopordized due to the singularities at the source points. However, ill-conditioning may occur if the source points are too far away from the boundary

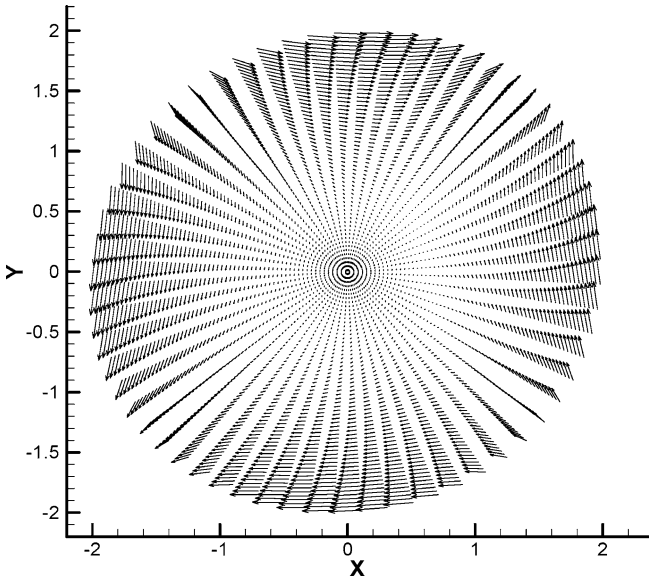

Fig. 7 The numerical solutions for the interior velocity vector

collocation points. In the next section the sensitivity of the accuracy due to the selection of the radius of the source points will be examined by using numerical experiments.

4 Results and discussion

The application of the MFS based on the Stokeslet for inverse boundary value problem should be tested to validate the present numerical scheme. As a first attempt, a two-dimensional inverse Stokes flow problem is considered. An inverse problem is an ill-posed problem wherein the boundaries of the computational domain are incomplete with respect to the specification of the boundary values of the flow variables. Let us consider an ill-posed problem consisting of an over-specified boundary (Γ_{I}) and an under-specified boundary (Γ_{II}) represented as

$$\partial\Gamma = \Gamma_{\mathrm{I}} + \Gamma_{\mathrm{II}} \tag{15}$$

We consider the specification of the velocities along with pressure or vorticity as over-specified boundary values on some part of the boundary, and specification of only one velocity component on the remaining part of the boundary as the under-specified boundary values. The boundary value problem results in an inverse Stokes problem. In addition many practical flow situations are inaccessible for the measurements of all the flow variables. The under- and over-specified boundaries themselves can be assumed to consist of a number of boundary segments. In some test cases of multiple boundary segments, two boundary segments are considered for the over-specified boundary Γ_{I} and three boundary segments for the under-specified boundary Γ_{II}.

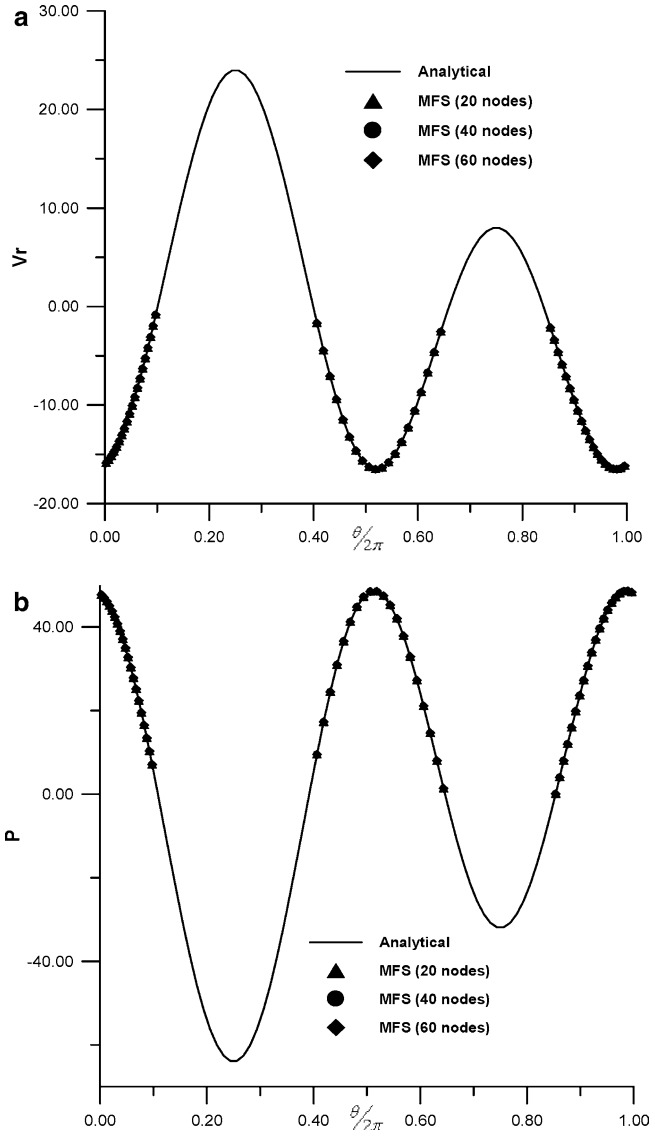

Fig. 8 Comparison with analytical solution and effect of number of boundary points on the results of **a** $v_{\mathrm{r}}|_{\Gamma_{\mathrm{II}}}$ and **b** $p|_{\Gamma_{\mathrm{II}}}$, on the under-specified boundary

In the following inverse Stokes problems, we consider the exact solutions of the velocity, pressure, vorticity, and stream function distributions by setting dynamic viscosity equal to unity as derived in the literature (Zeb et al. [11]):

Case 1:

$$\begin{cases} u = -x^2 + 4y^3 \\ v = 4x^3 + 2xy - 1 \\ p = 24xy - 2x \\ \zeta = 12x^2 + 2y - 12y^2 \\ \psi = -x^4 - x^2y + x + y^4 \end{cases} \tag{16}$$

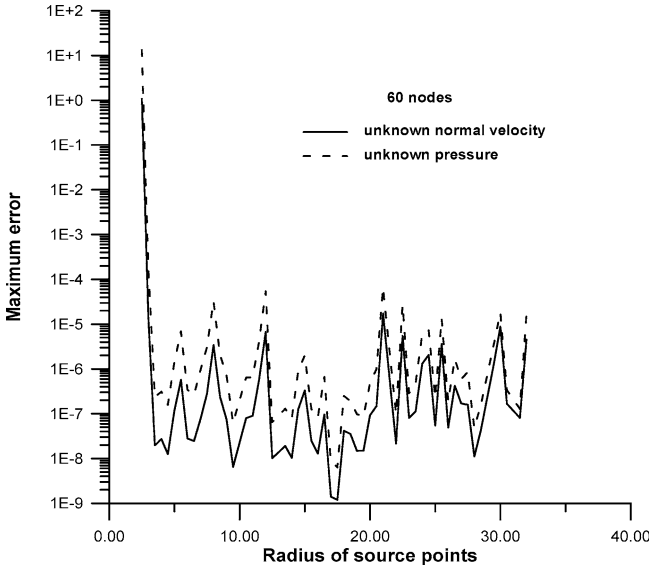

Fig. 9 Variation of maximum error with radius of source points for 60 boundary points

Case 2:

$$\begin{cases} v_r = \left(12 - r^2\right)\sin\theta + 2r\left(r^2 - 8\right)\cos 2\theta \\ v_\theta = \left(12 - 3r^2\right)\cos\theta - 4r\left(r^2 - 4\right)\sin 2\theta \\ p = 12r^2\cos 2\theta - 8r\sin\theta \\ \zeta = -\left(12r^{-1} + 5r\right)\cos\theta - 8\left(r^2 + 2\right)\sin 2\theta \\ \psi = \left(r^3 - 12r\right)\cos\theta + \left(r^4 - 8r^2\right)\sin 2\theta \end{cases} \tag{17}$$

where $x = r\cos\theta$ and $y = r\sin\theta$. When Eqs. (16) and (17) are imposed on the appropriate boundaries, they become the boundary conditions for the governing Stokes equations. Four numerical examples are undertaken, two inverse Stokes problems to validate the numerical scheme and the other two to demonstrate the effectiveness of the present scheme. The expressions given by Eqs. (16) and (17) are used as the boundary conditions for the problems discussed under cases 1 and 2 respectively in Sects. 4.1 and 4.2. For all the test cases discussed in the following sections, a smooth geometry of a circle of radius $R = 2$ is considered as the computational domain of the inverse Stokes problems.

4.1 Model validation

Case 1: single boundary segment

The over-specified computational boundary consists of a single boundary segment on which velocities and pressure are known. The under-specified boundary also composes a single segment on which only y-direction velocity is specified as follows:

$$u, v, \mathrm{p} \quad \text{on } \Gamma_{\mathrm{I}} \tag{18a}$$

$$v \quad \text{on } \Gamma_{\mathrm{II}} \tag{18b}$$

Zeb et al. [11] solved the previous problem using the BEM, while in the present work the MFS based on the Stokeslet is used to compute the radial and tangential velocity components $(v_{\mathrm{r}}, v_\theta)$. Referring to Fig. 1a, the over- and under-specified boundary portions Γ_{I} and Γ_{II} are chosen as

$$\Gamma_{\mathrm{I}} = \{(R,\theta) : 0 \le \theta \le (3\pi/2)\} \text{ and}$$

$$\Gamma_{\mathrm{II}} = \{(R,\theta) : (3\pi/2) \le \theta \le (2\pi)\} \tag{19}$$

Using the numerical procedure discussed in the previous section, the unknown field variables on the under-specified boundaries are computed first, and then compared with the analytical solutions. Figure 3a and b show the comparisons of radial velocity and pressure between the analytical solutions and the predicted boundary values, on the under-specified boundary region Γ_{II} using 20, 30, and 40 boundary points. Our predictions show excellent agreements with the analytical solutions for the radial velocity, as well as the pressure even with 20 coarse boundary points. It is also observed that the radial velocity and pressure on the

Table 2 Comparison with analytical solutions and effect of number of boundary points on v_{r} and P on under-specified boundary

$\theta/2\pi$	V_{r}				The unknown pressure (P)			
	Analytical	MFS (20 nodes)	MFS (40 nodes)	MFS (60 nodes)	Analytical	MFS (20 nodes)	MFS (40 nodes)	MFS (60 nodes)
0.01250	−15.17534	−15.17768	−15.17534	−15.17534	46.15369	46.16408	46.15369	46.15369
0.03750	−12.38854	−12.39036	−12.38854	−12.38854	39.03319	39.04113	39.03319	39.03319
0.06250	−8.25224	−8.25326	−8.25224	−8.25224	27.81819	27.82256	27.81819	27.81819
0.08750	−3.08386	−3.08406	−3.08386	−3.08386	13.43157	13.43306	13.43157	13.43157
0.43125	−7.04189	−7.04262	−7.04189	−7.04189	24.47495	24.47845	24.47495	24.47495
0.49375	−15.63660	−15.63891	−15.63660	−15.63660	47.22387	47.23439	47.22387	47.22387
0.55625	−14.93543	−14.93452	−14.93543	−14.93543	42.03736	42.03656	42.03736	42.03736
0.61875	−6.68575	−6.68438	−6.68575	−6.68575	14.62685	14.61954	14.62685	14.62685
0.86875	−4.61923	−4.61819	−4.61923	−4.61923	7.98312	7.97728	7.98312	7.98312
0.90625	−10.56750	−10.56537	−10.56750	−10.56750	27.25793	27.25003	27.25793	27.25793
0.94375	−14.93543	−14.93452	−14.93543	−14.93543	42.03736	42.03656	42.03736	42.03736
0.98125	−16.49822	−16.49912	−16.49822	−16.49822	48.55435	48.56245	48.55435	48.55435
Max.error (%)		2.34 E−02	3.29 E−07	1.02 E−08		1.05 E+00	2.67 E−06	1.19 E−07

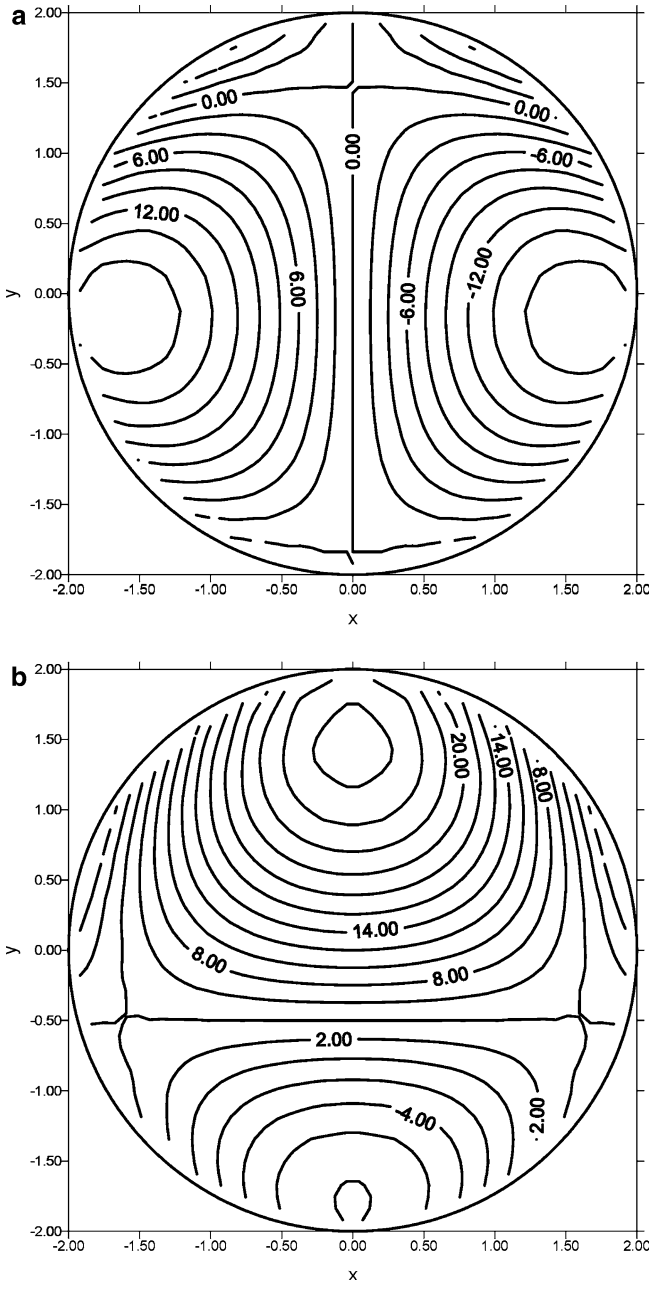

Fig. 10 The numerical results and corresponding analytical solutions for **a** the interior velocity (u) **b** the interior velocity (v)

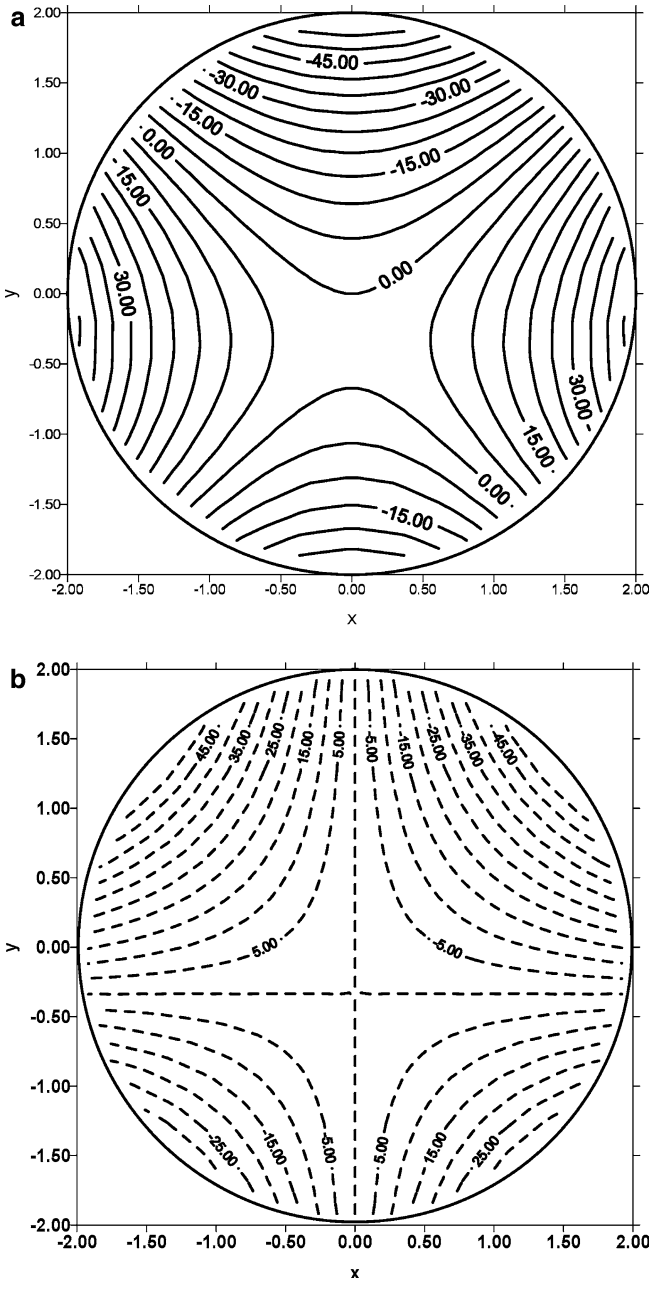

Fig. 11 The numerical results and corresponding analytical solutions for **a** the interior pressure (P) **b** the interior vorticity (ς)

predicted boundary are not sensitive for the range of the source points considered.

The effect of the number of source points on the accuracy of the numerical results in the inverse Stokes problem has also been carried out. For the purpose of comparison, the radial velocity and pressure on the under-specified boundary are considered. In Table 1 the numerical results and corresponding analytical solutions are compared. The tabulated values indicate that the maximum error decreases with an increase in the number of source points. The above comparisons clearly demonstrate that, if we take 40 source points the proposed form of the MFS can be utilized to solve inverse problems with accuracy close to the analytical solutions.

In the MFS, the distance of the source point from the field point has some influence on the solution accuracy and ill-condition of the equations. A study was conducted with 40 source points to determine the range of the radius of source points, with the results shown in Fig. 4. This figure agrees with the MFS theory that the system becomes singular when the source points are too close to the boundary, and is ill-conditioned when they are too far from each other. However in the inverse problems considered in the present work, there is a wide

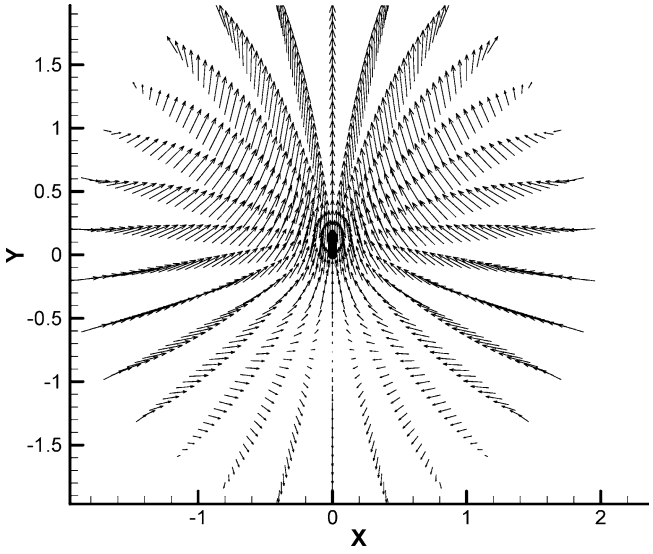

Fig. 12 The numerical solutions for the interior velocity vector

range of source points in which generally good results can be obtained.

Figure 5a and b exhibit the interior x-direction velocity distributions and the interior y-direction velocity distributions respectively in the circular cavity. The shape of these contours is as expected. Figure 6a and b show the distributions of pressure and vorticity at the interior region of the cavity. The present method can predict a smooth pressure variation as observed from Fig. 6a.

Another important verification for the proposed numerical scheme is the velocity vector plot at the interior of the circular domain. If the predictions of the velocities on the under-specified boundary are incorrect, then the governing equation will not be satisfied at the under-specified boundary, resulting in a non-physical behavior of the system. The velocity vector distributions at the interior region of the cavity shown in Fig. 7 clearly confirm that the predicted boundary velocities are physically feasible.

Case 2: multiple boundary segments

In many practical flow situations, the over-specified and under-specified boundaries may consist of a number of small boundary segments. For the circular cavity discussed in the above section, the over- and under-specified boundary conditions are assumed to be a combination of 5 small boundary segments. They are represented as follows:

$$u, v, p \quad \text{on } \Gamma_{\mathrm{I}} = \Gamma_2 \cup \Gamma_4 \tag{20a}$$

$$v \quad \text{on } \Gamma_{\mathrm{II}} = \Gamma_1 \cup \Gamma_3 \cup \Gamma_5 \tag{20b}$$

where

$$\Gamma_1 = \{(R,\theta) : 0 \le \theta \le 0.2\pi\},$$
$$\Gamma_2 = \{(R,\theta) : 0.2\pi \le \theta \le 0.8\pi\},$$
$$\Gamma_3 = \{(R,\theta) : 0.8\pi \le \theta \le 1.3\pi\},$$
$$\Gamma_4 = \{(R,\theta) : 1.3\pi \le \theta \le 1.7\pi\},$$
$$\Gamma_5 = \{(R,\theta) : 1.7\pi \le \theta \le 2\pi\}.$$

Table 3 Comparison with analytical solutions and effect of number of boundary points on v_r and vorticity ζ on under-specified boundary

	$\theta/2\pi$	Analytical	MFS (20 nodes)	MFS (30 nodes)	MFS (40 nodes)
V_r	0.76250	−0.88416	−0.88491	−0.88416	−0.88416
	0.78750	−4.57658	−4.57975	−4.57658	−4.57658
	0.81250	−8.00087	−8.00087	−8.00087	−8.00087
	0.83750	−10.93521	−10.93204	−10.93521	−10.93521
	0.86250	−13.13414	−13.13338	−13.13414	−13.13414
	0.88750	−14.34648	−14.34573	−14.34648	−14.34648
	0.91250	−14.35087	−14.34770	−14.35087	−14.35087
	0.93750	−13.00295	−13.00296	−13.00295	−13.00295
	0.96250	−10.28399	−10.28716	−10.28399	−10.28399
	0.98750	−6.33852	−6.33927	−6.33852	−6.33852
	Max.error (%)		3.17 E−01	5.62 E−07	1.30 E−07
The unknown vorticity, (ζ)	0.04167	42.60450	42.58611	42.60450	42.60450
	0.12500	2.82843	2.82843	2.82843	2.82843
	0.20833	−37.70552	−37.68713	−37.70552	−37.70552
	0.29167	−37.70552	−37.72390	−37.70552	−37.70552
	0.37500	2.82843	2.82843	2.82843	2.82843
	0.45833	42.60450	42.62288	42.60450	42.60450
	0.54167	40.53394	40.51556	40.53394	40.53394
	0.62500	−2.82843	−2.82843	−2.82843	−2.82843
	0.70833	−45.43292	−45.41454	−45.43292	−45.43292
	0.79167	−45.43292	−45.45130	−45.43292	−45.43292
	0.87500	−2.82843	−2.82841	−2.82843	−2.82843
	0.95833	40.53394	40.55232	40.53394	40.53394
	Max.error (%)		1.84 E+00	4.06 E−06	1.30 E−06

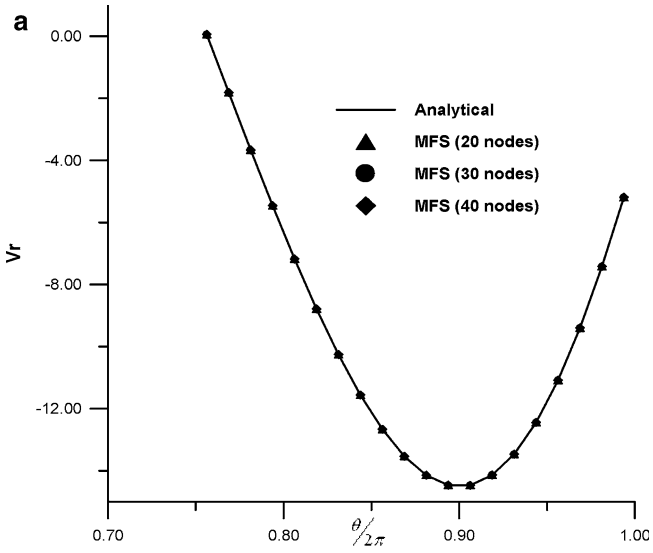

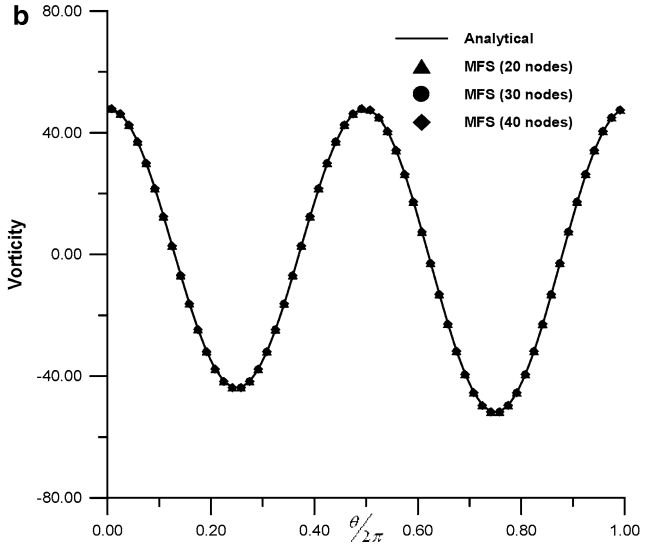

Fig. 13 Comparison with analytical solutions and effect of number of boundary points on the results of **a** $v_r|_{\Gamma_{II}}$ and **b** $\zeta|_\Gamma$, on the under-specified boundary

Numerical results for the velocities and pressure on the under-specified boundary are computed. Figure 8a and b show the comparisons of radial velocity and pressure between the analytical solutions and the present results on the under-specified boundary using 20, 40, and 60 source points. As seen from the above figures, the results obtained by the present numerical scheme of the MFS based on the Stokeslet show excellent agreement with the analytical solutions for both the velocity and pressure. It is to be noted that the smooth variation of pressure has been correctly predicted by the MFS. The effects of the numbers of boundary points on the accuracy of the flow variables are observed by the fact that with increase in number of boundary nodes the accuracy of numerical prediction increases, as shown in Table 2. It is worthwhile noting that as the number of segments

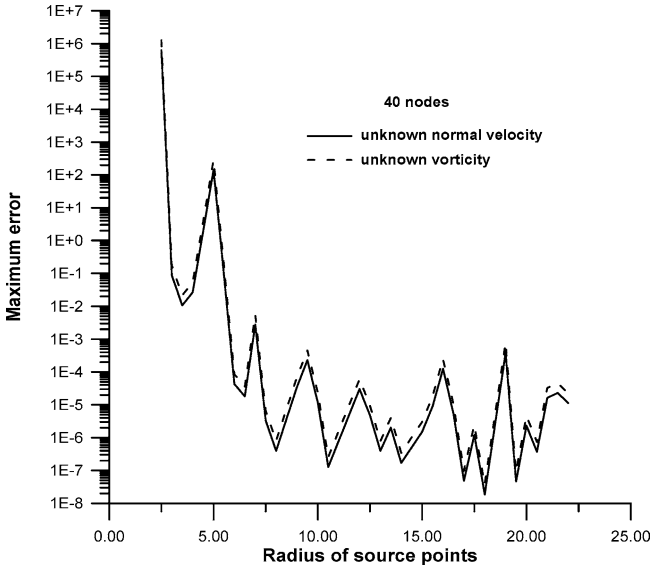

Fig. 14 Variation of maximum error with radius of source points for 40 boundary points

of the under- and over-specified boundaries increases, the number of boundary points has to be increased in order to obtain accurate results.

The effect of the radius of the source points on the accuracy of numerical predictions is studied using 60 boundary points. Figure 9 shows the relationship between the radius of the source points and the maximum error. This figure also agrees with the theoretical predications, and has a wide range of radius for the source points in which the results with high accuracy can be obtained. Figure 10a and b depict the distributions of the interior x-direction and y-direction velocities in the circular cavity respectively. Since the flow variables on the under-specified boundary are computed correctly, the velocities at the interior region of the cavity also could be predicted accurately as demonstrated by the expected trends shown in the above figures. The distributions of pressure and vorticity at the interior region of the cavity are shown in Fig. 11a and b respectively. Figure 11 demonstrates the orthogonal trajectories between the pressure and vorticity contours. The vorticity is generated only at the cavity boundary, and this trend is correctly predicted by the present numerical scheme as seen from the Fig. 11b. Figure 12 shows the velocity vector distributions inside the circular cavity as predicted by the present numerical scheme. As expected the stagnation points noticed in Fig. 12 agree with those observed in Figs. 10 and 11.

4.2 Model applications

Case 1: single boundary segment

After validating the proposed numerical scheme based on the MFS, the study was extended to solve two new

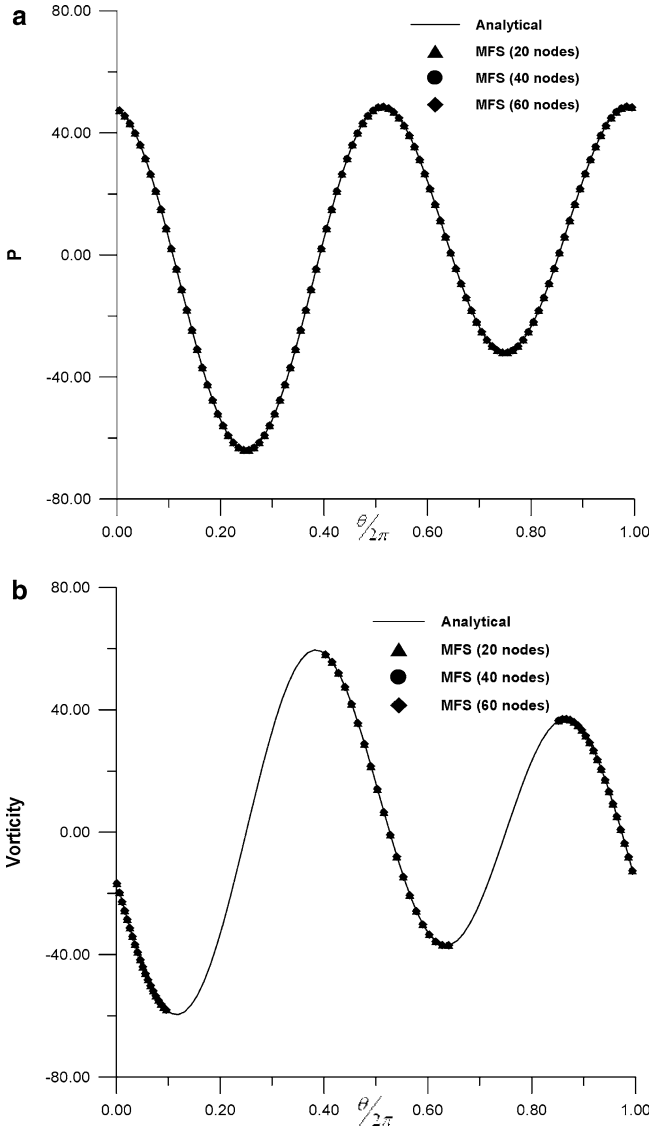

Fig. 15 Comparison with analytical solutions and effect of number of boundary points on the results of **a** $p|_{\Gamma}$ and **b** $\varsigma|_{\Gamma_{II}}$, on the under-specified boundary

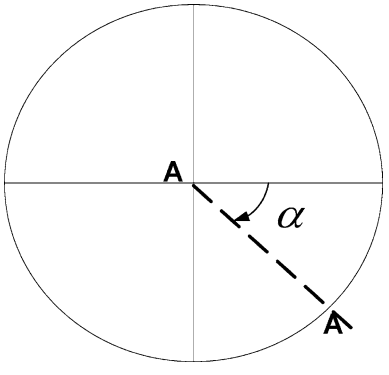

Fig. 16 Definition of section A-A $\left(\alpha = \frac{\pi}{4}\right)$

boundary inverse problems with different over-specified boundary values on different numbers of boundary segments. Pressure is an important flow variable in the

Table 4 Comparison with analytical solutions and effect of number of boundary points on v_r and v_θ on section A-A

Radius	The velocity v_r in section A-A				The velocity v_θ in section A-A			
	Analytical	MFS (20 nodes)	MFS (40 nodes)	MFS (60 nodes)	Analytical	MFS (20 nodes)	MFS (40 nodes)	MFS (60 nodes)
0.1	−8.47821	−8.47654	−8.47821	−8.47821	6.86807	6.86719	6.86807	6.86807
0.3	−8.42164	−8.41991	−8.42164	−8.42164	3.60236	3.60313	3.60236	3.60236
0.5	−8.30850	−8.30677	−8.30850	−8.30850	0.45495	0.45741	0.45495	0.45495
0.7	−8.13880	−8.13722	−8.13880	−8.13880	−2.38217	−2.37809	−2.38217	−2.38217
0.9	−7.91252	−7.91138	−7.91252	−7.91252	−4.71699	−4.71150	−4.71699	−4.71699
1.1	−7.62968	−7.62934	−7.62968	−7.62968	−6.35752	−6.35101	−6.35752	−6.35752
1.3	−7.29027	−7.29114	−7.29027	−7.29027	−7.11175	−7.10486	−7.11175	−7.11175
1.5	−6.89429	−6.89671	−6.89429	−6.89429	−6.78769	−6.78137	−6.78769	−6.78769
1.7	−6.44174	−6.44573	−6.44174	−6.44174	−5.19333	−5.18889	−5.19333	−5.19333
1.9	−5.93263	−5.93670	−5.93263	−5.93263	−2.13669	−2.13587	−2.13669	−2.13669
Max.error (%)		5.43 E−02	5.63 E−06	1.74 E−07		5.43 E−01	6.52 E−06	1.97 E−07

analysis of computational fluid dynamics (CFD) applications. Though it is easy to measure the value of pressure inside a fluid domain, it may not be always possible to get the correct pressure values at all the points of the boundaries. With the assumption that the pressure is known only at one point of the computational boundary, the inverse Stokes flow is solved for the flow variables. The computational boundary is assumed to be the same as in the validation case 1. The boundary values for these over- and under-specified boundaries are specified as follows:

u, v, p on Γ_{I} pressure known only at one point on this boundary (21a)

v on Γ_{II} (21b)

Figure 13a and b show the comparisons of the velocity and vorticity distributions between the analytical solutions and the present results on the under-specified boundary using 20, 30, and 40 boundary points. It is observed that the present numerical scheme is capable of predicting the flow variables with accuracy close to the analytical solutions. The results on the effect of number of boundary nodes on the numerical accuracy are tabulated in Table 3. These results indicate that the numerical accuracy of the MFS increases with an increase in the number of boundary points. Figure 14 shows the effect of radius of source points on the maximum error in numerical predictions by the MFS. In this case a wide range of radius of source points is also observed. Excellent agreement of the present results with the analytical solutions indicate that the present numerical scheme based on the MFS could predict the flow variables accurately on the under-specified boundaries in accordance with the physics underlying the problem.

Case 2: multiple boundary segments

In this last case, instead of pressure we assume only vorticity values are known on part of the boundary. This problem resembles the validation case 2, in which the over-specified boundary consists of two segments and the under-specified boundary includes three segments. The flow results for this case are obtained using the following boundary conditions:

u, v, ζ on $\Gamma_{\mathrm{I}} = \Gamma_2 \cup \Gamma_4$ (22a)

v on $\Gamma_{\mathrm{II}} = \Gamma_1 \cup \Gamma_3 \cup \Gamma_5$. (22b)

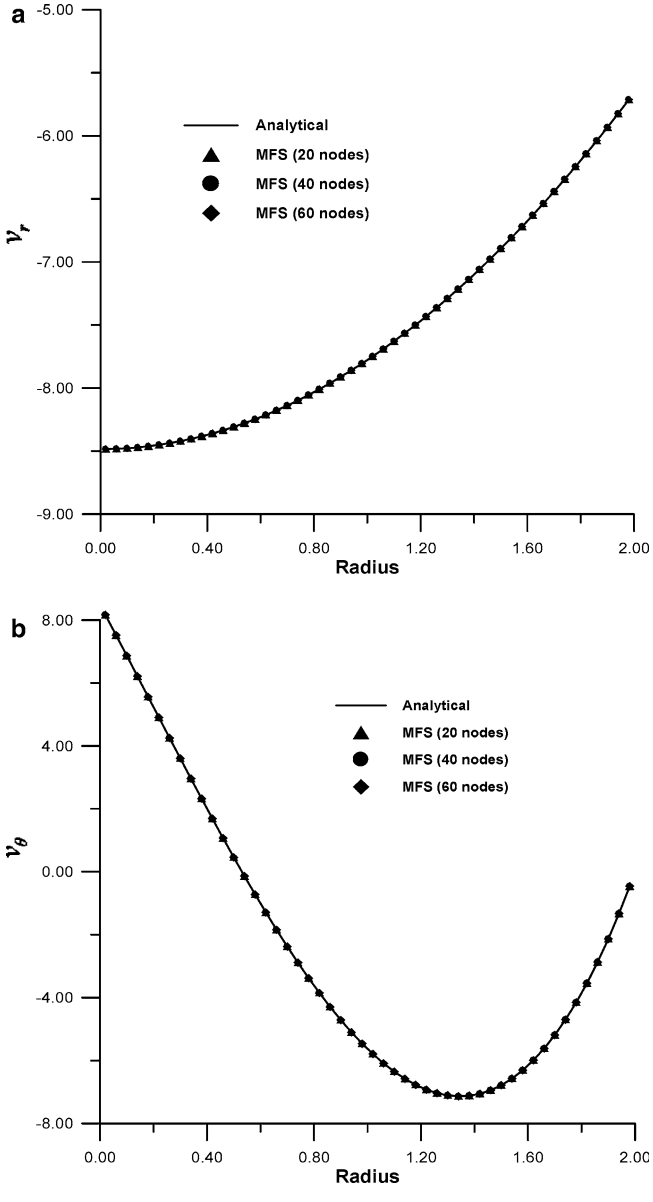

Fig. 17 Comparison with analytical solutions and effect of number of boundary points on the results of **a** (v_r) and **b** (v_θ), in section A-A

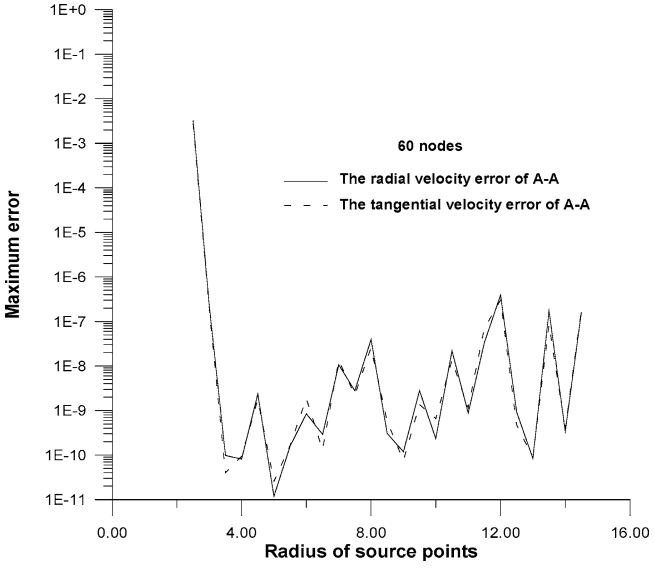

Fig. 18 Variation of maximum error with radius of source points for 60 boundary points

Figure 15a and b represent the comparisons for the pressure and vorticity values between the analytical solutions and the present results on the under-specified boundary using 20, 40, and 60 boundary points. Figure 17a and b show the comparisons for the radial and tangential velocities between the analytical solutions and the present results obtained with three different number of boundary nodes on the section A-A as defined in Fig. 16. The velocities predicted by the MFS are in agreement with the analytical solutions. In Table 4, we describe the effect of the number of boundary nodes on the numerical accuracy of the tangential and radial velocities on the under-specified boundary. As seen from the above tables, the more the number of boundary nodes, the higher the accuracy of the numerical predictions. Figure 18 shows the effect of the radius of source points on the maximum error in the predictions of both the radial and tangential velocities. This figure also indicates a wide range of radius for the source points in which accurate results can be obtained.

In general the matrix equations obtained by the MFS are ill-conditioned depending upon the type of problem being solved and sometimes a regularization technique needs to be employed. In the present method, however it is observed that there exists a wide range of radius of source points (Figs. 4, 9, 14 and 18), in which the numerical predictions are in close agreement with available analytical solutions. Hence it was numerically found that the problem of ill-condition did not pose any difficulty in getting the solutions for the inverse Stokes problems discussed in this article. The various numerical experiments performed using different combinations of flow variables on the under- and over-specified boundaries have demonstrated that the present numerical scheme based on the MFS is a potentially useful tool for directly solving inverse Stokes problems.

5 Conclusions

The MFS has been employed to solve boundary inverse Stokes flow in a circular cavity using the Stokeslet as source points. All the boundary values on the over- and under-specified boundary segments have been used to determine the coefficients of the fundamental solutions. Four types of inverse problems have been obtained, assuming different combination of velocities and pressure as unknown variables on different number of boundary segments for over- and under-specified boundaries. The numerical predictions of the velocity, pressure and vorticity fields on the under-specified boundary segments are in close agreement with the available analytical solutions for all the test problems. An experimental investigation of numerical errors shows that the accuracy of numerical prediction of the field variables improves with increasing number of source points. When the number of boundary segments of over- and under-specified boundary conditions increases, the number of collocation points was also increased for better results. For each of the test cases considered in this work, there exists a wide range of radius of source points in which the numerical results close to the analytical solution could be obtained without problems of ill-conditioning. The numerical results predicted for all the test cases indicate that the proposed method is a promising numerical tool to solve inverse Stokes flow problems without using any iterative or regularization procedure.

Acknowledgements The National Science Council of Taiwan is gratefully acknowledged and appreciated for providing financial support to carry out the present work under the Grant No. NSC 93-2611-E-002-001 and No. NSC 94-2211-E-464-001. Our special thanks are extended to the editor Prof. S.L. Crouch and reviewers for constructive suggestions.

References

1. Fairweather G, Karageorghis A (1998) The method of fundamental solutions for elliptic boundary value problems. Adv Comput Math 9:69–95
2. Fairweather G, Karageorghis A, Martin PA (2003) The method of fundamental solutions for scattering and radiation problems. Eng Anal Bound Elem 27:759–769
3. Golberg MA, Chen CS (1998) The method of fundamental solutions for potential, Helmholtz and diffusion problems. Boundary Integral Methods: Numerical and Mathematical Aspects, (ed) Golberg MA, WIT Press/Computational Mechanics Publications, Boston, pp 103–176
4. Golberg MA (1995) The method of fundamental solutions for Poisson's equation. Eng Anal Bound Elem 16:205–213
5. Tsai CC, Young DL, Cheng AH-D (2002) Meshless BEM for three-dimensional Stokes flows. Comput Modeling Eng Sci 3:117–128
6. Tsai CC (2002) Meshless numerical methods and their engineering applications. PhD Thesis, Department of Civil Engineering, National Taiwan University, Taipei, Taiwan
7. Alves CJS, Silvestre AL (2004) Density results using Stokeslets and a method of fundamental solutions for the Stokes problems. Eng Anal Bound Elem 28:1245–1252
8. Agoshkov V, Bardos C, Buleev S (2002) Solution of the Stokes problem as an inverse problem. Comput Meth Appl Math 3:213–232
9. Farcas A, Elliott L, Ingham DB, Lesnic D, Mera NS (2003) A dual reciprocity boundary element method for the regularized numerical solution of the inverse source problem associated to the Poisson equation. Inverse Problem in Eng 11:123–139
10. Zeb A, Elliott L, Ingham DB, Lesnic D (2002) An inverse Stokes problem using interior pressure data. Eng Anal Bound Elem 26:739–745
11. Zeb A, Elliott L, Ingham DB, Lesnic D (2000) Boundary element two-dimensional solution of an inverse Stokes problem. Eng Anal Bound Elem 24:75–88
12. Marin L, Lesnic D (2004) The method of fundamental solutions for the Cauchy problem in two-dimensional linear elasticity. Int J Solids Struct 41:3425–3438
13. Marin L (2005) A meshless method for the numerical solution of the Cauchy problem associated with three-dimensional Helmholtz-type equations. Appl Math Comput 165: 355–374
14. Pozrikidis C (1992) Boundary integral and singularity methods for linearized viscous flow. Cambridge University Press, Cambridge